Kinetics of Factor Xa Inhibition by Recombinant Tick Anticoagulant Peptide: Both Active Site and Exosite Interactions Are Required for a Slow- and Tight-Binding Inhibition Mechanism†

Alireza R. Rezaie*

Edward A. Doisy Department of Biochemistry and Molecular Biology, Saint Louis University School of Medicine, St. Louis, Missouri 63104

Received December 3, 2003; Revised Manuscript Received January 22, 2004

ABSTRACT: Recombinant tick anticoagulant peptide (rTAP) is a competitive slow- and tight-binding inhibitor of factor Xa (FXa) with a reported equilibrium dissociation constant (K_I) of ∼0.2 nM. The inhibitory characteristics and the high selectivity of rTAP for FXa are believed to arise from the ability of the inhibitor to specifically interact with the residues of both the active site as well as those remote from the active site pocket of the protease. To localize the rTAP-interactive sites on FXa, the kinetics of inhibition of wild-type and 18 different mutants of recombinant FXa by the inhibitor were studied by either a discontinuous assay method employing the tight-binding quadratic equation or a continuous assay method employing the slow-binding kinetic approach. It was discovered that K_I values for the interaction of rTAP with four FXa mutants (Tyr^{99} → Thr, Phe^{174} → Asn, Arg^{143} → Ala, and a Na^+-binding loop mutant in which residues 220−225 of FXa were replaced with the corresponding residues of thrombin) were elevated by 2−3 orders of magnitude for each mutant. Further studies revealed that the characteristic slow type of inhibition by rTAP was also eliminated for the mutants. These findings suggest that the interaction of rTAP with the P2-binding pocket, the autolysis loop, and the Na^+-binding loop is primarily responsible for its high specificity of FXa inhibition by a slow- and tight-binding mechanism.

Factor Xa (FXa)[1] is the vitamin K-dependent serine protease of the prothrombinase complex (FXa, factor Va, negatively charged membrane, and calcium) which is responsible for the conversion of prothrombin to thrombin in the final stage of the coagulation cascade (*1*, *2*). The proteolytic activity of FXa in plasma is regulated by three physiological inhibitors, antithrombin (*3*, *4*), protein Z-dependent protease inhibitor (ZPI) (*5*), and tissue factor pathway inhibitor (TFPI) (*6*). The first two inhibitors belong to the serpin family of plasma inhibitors, both of which require cofactors for their effective interaction with FXa. Thus, the interaction of AT with the heparin-like glycosaminoglycans on the surface of the endothelium (*3*, *7*) and formation of the ZPI complex with protein Z on membrane phospholipids (*5*) are required for the physiological regulation of FXa by both serpins. On the other hand, TFPI is a slow- and tight-binding, Kunitz-type inhibitor that is capable of rapidly inhibiting FXa independent of a cofactor (*8*). The molecular basis for an effective cofactor-independent inhibition of FXa by TFPI is believed to lie in the ability of the inhibitor to make extensive interactions with both the active site and secondary binding sites (exosites) remote from the active site pocket of the protease (*9*). This type of interaction also accounts for the ability of TFPI to inhibit FXa by a slow- and tight-binding inhibition mechanism (*8*).

In addition to TFPI, a number of nonphysiological but naturally occurring peptide inhibitors specific for FXa have recently been identified which inhibit the protease by a similar slow- and tight-binding inhibition mechanism (*10*, *11*). The interaction of a recombinant form of such an inhibitor possessing potent antithrombotic properties, derived from the soft tick *Ornithodoros moubata* [recombinant tick anticoagulant peptide (rTAP)], with FXa has been extensively studied (*10*−*14*). The kinetic data have indicated that rTAP competitively inhibits FXa with an equilibrium dissociation constant of ∼0.2 nM (*12*). A detailed kinetic analysis employing rapid kinetic methods has also revealed that rTAP inhibits FXa by a two-step interaction mechanism in which a reversible inhibitor−protease complex that formed in the first step is then isomerized to a tight complex at a high rate constant (k_2) of 123 s^{-1} in the second step of the interaction (*13*). Recently, the X-ray crystal structure of rTAP in complex with bovine FXa was determined (*15*). The structural data together with the mutagenesis data indicated that, like TFPI, in addition to binding to the active site pocket of FXa, the inhibitor also interacts with exosites remote from the catalytic pocket of the protease (*9*, *15*). Thus, it was demonstrated that the three N-terminal residues (Tyr^1, Asn^2, and Arg^3) of rTAP occupy the active site pocket of FXa in

† The research discussed herein was supported by grants awarded by the National Heart, Lung, and Blood Institute of the National Institutes of Health (Grants HL 62565 and HL 68571 to A.R.R.).

* To whom correspondence should be addressed: Department of Biochemistry and Molecular Biology, Saint Louis University School of Medicine, 1402 S. Grand Blvd., St. Louis, MO 63104. Phone: (314) 977-9240. Fax: (314) 977-9205. E-mail: rezaiear@slu.edu.

[1] Abbreviations: FXa, factor Xa; GD-FXa, Gla domain-less factor Xa; rTAP, recombinant tick anticoagulant peptide; TFPI, tissue factor pathway inhibitor; SpFXa, Spectrozyme FXa; SpPCa, Spectrozyme PCa.

10.1021/bi036177y CCC: $27.50
Published on Web 03/02/2004

such a way that P1 Tyr^{1} binds to the S1 pocket [nomenclature of Schechter and Berger (*16*)] and P3 Arg^{3} extends toward the S2−S4 aryl binding pocket of the protease (*15*). In this pocket, the guanidinium group of P3 Arg^{3} appears to form a salt bridge with Glu^{97} [chymotrypsinogen numbering system used throughout (*17*)], and its hydrophobic side chain interacts with hydrophobic residues of the aryl binding pocket, composed of Tyr^{99}, Phe^{174}, and Trp^{215}, to stabilize the inhibitor in the active site pocket of FXa (*15*). Structural data further suggest that two acidic regions on the C-terminal helix of rTAP make extended interactions with the basic residues of the autolysis loop and the sodium-binding 220−225 loop (residues 220−225) of bovine FXa (*15*, *18*). A leech inhibitor, termed hirudin, is also known to interact with thrombin by a similar mechanism, with the N-terminal residues of the inhibitor binding to the active site pocket and the acidic C-terminal residues interacting with a basic anion binding exosite of the protease (*19*−*21*).

To understand the mechanism by which rTAP inhibits human FXa with a high degree of specificity, the kinetics of inhibition of 18 mutants of FXa by the inhibitor were studied. The mutant constructs were prepared rationally on the basis of known X-ray crystal structures, and they contained substitutions on several surface loops of FXa, including residues in 39, 60, 99, 148, and sodium-binding loops, all of which are known to play critical roles in determining the macromolecular substrate and inhibitor specificity of coagulation proteases (*22*, *23*). The ever-growing body of evidence in the literature suggests that the variant residues of these conserved surface loops make a marked contribution to the cofactor-dependent recognition and assembly of coagulation activation complexes on membrane surfaces (*24*−*29*). In addition to the surface loop mutants, several other FXa mutants were prepared that contained substitutions in the subsite residues of the catalytic pocket which are known to be critical for determining the P3−P3′ binding specificity of coagulation proteases (*30*, *31*). The kinetics of inhibition of wild-type and mutant FXa derivatives were measured by both discontinuous and continuous assay methods, and the kinetic data were analyzed by either the tight-binding quadratic equation or the slow-binding kinetic approach as described previously (*32*). It was discovered that the interaction of rTAP with Arg^{143} of the autolysis loop, basic residues of the sodium-binding 220−225 loop, and Tyr^{99} and Phe^{174} of the aryl binding pocket is essential for the inhibition of FXa by rTAP by a slow- and tight-binding inhibition mechanism. This was evidenced by the observation that the mutagenesis of any one of these residues not only dramatically impaired the equilibrium dissociation constants for the rTAP interaction with the FXa mutants but also abolished the characteristic slow- and tight-binding interaction of the inhibitor with the mutant proteases.

MATERIALS AND METHODS

Construction, Mutagenesis, and Expression of Recombinant Proteins. The construction and expression of recombinant wild-type factor X (FX) in both full-length and Gla domain-less forms (GD-FX) in human embryonic kidney 293 cells have been described previously (*33*, *34*). The FX mutants, into which Glu^{36} → Gln (E36Q), Glu^{37} → Gln (E37Q), Glu^{39} → Gln (E39Q), Gln^{61} → Ala (Q61A), Lys^{62} → Glu (K62E), Arg^{63} → Glu (R63E), and Glu^{97} → Ala (E97A) mutations were introduced, were constructed by PCR mutagenesis methods and expressed in the same vector system described above. The Na^{+}-binding loop mutant of FX in the GD-FX form, in which Ala^{221} and Lys^{223} were replaced with two Asp residues found at the corresponding sites of thrombin, was prepared by the same methods and expressed in the same expression and purification vector system described above. The substitution of these two residues results in an FX mutant ($220-225^{Th}$) in which the 220−225 loop of the protease is identical to the corresponding sequence of thrombin. Unlike FXa, thrombin is not inhibited by rTAP (*10*). The accuracy of all constructs was confirmed by DNA sequencing prior to their expression in mammalian cells. The construction, expression, and characterization of the autolysis loop mutants of FX, including Arg^{143} → Ala (R143A), Lys^{147} → Ala (K147A), Arg^{150} → Ala (R150A), and Arg^{154} → Ala (R154A), have been described previously (*34*). The construction, expression, and characterization of the Gln^{192} → Glu (Q192E), Tyr^{99} → Thr (Y99T), and Phe^{174} → Asn (F174N) mutants in GD-FX forms have also been described previously (*31*, *35*). All mutants were purified to homogeneity, activated by the FX activating enzyme from Russell's viper venom (RVV-X), and active site titrated with known concentrations of antithrombin as described previously (*31*, *34*).

Human plasma FXa and RVV-X were purchased from Haematologic Technologies Inc. (Essex Junction, VT). Recombinant tick anticoagulant peptide (rTAP) was a generous gift from G. Vlasuk (CORVAS International Inc., San Diego, CA). The chromogenic substrates, Spectrozyme FXa (MeO-CO-D-CHG-Gly-Arg-pNA·AcOH) (SpFXa), and Spectrozyme PCa (H-D-Lys(γ-Cbo)-Pro-Arg-pNA·2AcOH) (SpPCa) were purchased from American Diagnostica (Greenwich, CT), and S2765 (*N*-α-Z-D-Arg-Gly-pNA·2HCl) was purchased from Kabi Pharmacia/Chromogenix (Franklin, OH).

Inhibition Assays. The ability of FXa derivatives to interact with rTAP was evaluated by both discontinuous and continuous assay methods as described previously (*12*, *36*). In the discontinuous assay method, FXa (0.5 nM) was incubated with different concentrations of rTAP (0.3−15 nM) in 0.1 M NaCl and 0.02 M Tris-HCl (pH 7.5) containing 0.1 mg/mL bovine serum albumin, 0.1% polyethylene glycol 8000, and 5 mM Ca^{2+} (TBS/Ca^{2+}) in 80 μL volumes in 96-well polystyrene assay plates. Following incubation for 30 min at room temperature (a time period determined to be sufficient for the establishment of equilibrium), 20 μL of SpFXa was added to a final concentration of 200 μM, and the K_I values were estimated by nonlinear regression analysis of data using eq 1, for the tight-binding inhibitors as described previously (*30*, *32*).

$$V_s/V_o = \{E_o - I_o - K_I + [(E_o + I_o + K_I)^2 - 4E_oI_o]^{1/2}\}/2E_o \quad (1)$$

where V_s and V_o are the steady-state velocities of chromogenic substrate hydrolysis in the presence and absence of rTAP, respectively, E_o and I_o are the total concentrations of FXa and rTAP, respectively, and K_I is the inhibition constant.

The K_I values for certain FXa mutants, which exhibited a dramatic impairment of the interaction with rTAP and interacted reversibly with the inhibitor, were determined at

Scheme 1

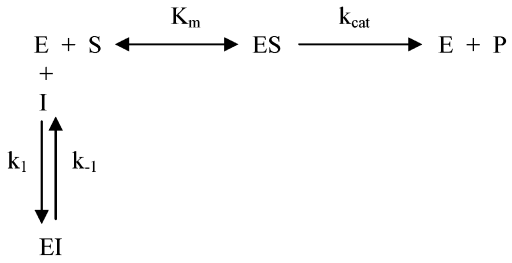

Scheme 2

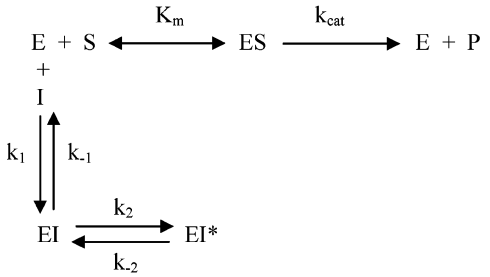

equilibrium under pseudo-first-order conditions (the minimum concentration of rTAP was in excess of the FXa concentration by at least 10-fold) by nonlinear regression analysis of data according to eq 2 as described previously (*30*).

$$V_s = V_o/\{I_o/[K_I(1 + [S]/K_m)] + 1\} \quad (2)$$

where [S] is the chromogenic substrate concentration and K_m is the Michaelis−Menten constant for the hydrolysis of the chromogenic substrate by the FXa mutant.

Slow-Binding Kinetics. The ability of FXa derivatives to bind rTAP was also evaluated by the slow-binding kinetic approach as described by Morrison and Walsh (*32*). In this case, a series of inhibition progress curves for each derivative were generated by adding 0.1 nM enzyme (final concentration for all derivatives with the exception of 5 nM for the 220−225Th mutant) to wells of a 96-well plate containing various concentrations of rTAP (from 1 nM to 10 μM) and 200−400 μM SpFXa or SpPCa (for the T99Y and F174N mutants) in the same TBS buffer system described above. The cleavage of the chromogenic substrate by FXa was assessed continuously for up to 2 h at room temperature. Data from each curve at different concentrations of the inhibitor were fitted by nonlinear regression analysis to the integrated rate equation (eq 3) for the slow-binding inhibitors as described previously (*32*).

$$A = v_s t + (v_o - v_s)(1 - e^{-k_{obs}t})/k_{obs} + A_o \quad (3)$$

where A is the absorbance at 405 nm at time t, v_o and v_s are the initial and final steady-state velocity, respectively, k_{obs} is the apparent first-order rate constant, and A_o is the initial absorbance at 405 nm. Computer fitting of data estimated values for v_o, v_s, k_{obs}, and A_o. These values were analyzed by different methods to obtain reaction rate constants and K_I values for the interaction of rTAP with each FXa derivative according to either Scheme 1 or Scheme 2, depending on the observed inhibition mechanism (*32*, *37*). Scheme 1 predicts that the k_{obs} values, as determined by eq 3, will increase linearly with the inhibitor concentration, and thus, the association rate constant, k_1 (k_{on}), and the dissociation rate constant, k_{-1} (k_{off}), and K_I can be calculated from eqs 4 and 5. Scheme 2, on the other hand, predicts that k_{obs} values will increase hyperbolically with the inhibitor concentration, and the values of k_2, k_{-2}, the initial K_i, and the final K_I can be estimated from eqs 6 and 7 (*32*, *37*).

$$k_{obs} = k_{-1} + k_1[I]/(1 + [S]/K_m) \quad (4)$$

$$K_I = k_{-1}/k_1 \quad (5)$$

$$k_{obs} = k_{-2} + k_2[I]/[[I] + K_i(1 + [S]/K_m)] \quad (6)$$

$$K_I = K_i[k_{-2}/(k_2 + k_{-2})] \quad (7)$$

The Gibbs standard free energy change ($\Delta G°_b$) for formation of the FXa−rTAP complex was also calculated from the values of K_I using the equation $\Delta G°_b = RT \ln K_I$, where R is the gas constant and T is the absolute temperature (in kelvin). The difference in binding energy between the wild type and FXa mutants (wild-type $\Delta G°_b$ minus mutant $\Delta G°_b$) was denoted as $\Delta\Delta G°_b$.

Data Analysis. The Enzfitter computer program (R. J. Leatherbarrow, Elsevier, Biosoft) was used to fit the kinetic data to the appropriate equations presented above. All measurements are averages of at least two to three independent measurements ± the standard error.

RESULTS

Expression and Purification and Activation of Recombinant Proteins. Both the wild type and mutant FX derivatives were expressed in the expression and purification vector systems described previously (*33*, *34*). The mutant proteins were purified to homogeneity by a combination of immunoaffinity and ion exchange chromatography using the monoclonal antibody HPC4 and a Mono Q column (*34*). SDS−PAGE analysis of all FX derivatives suggested that the recombinant proteins have been purified to homogeneity and that they all migrate with molecular masses similar to that of the plasma-derived FX (data not shown). All derivatives could be converted to their active forms by RVV-X as determined by an amidolytic activity assay using SpFXa or S2765. Following activation, the concentrations of FXa derivatives were determined by both an amidolytic activity assay and active site titration with known concentrations of antithrombin (*33*, *34*). All mutants, with the exception of the 220−225Th mutant, exhibited normal amidolytic activity, suggesting that the mutagenesis did not adversely affect the folding or the reactivity of the catalytic pocket of the mutant proteases. Relative to the cleavage rate of S2765 by wild-type FXa (K_m = 50 μM and k_{cat} = 240 s^{-1}), the catalytic activity of 220−225Th toward the chromogenic substrate was dramatically impaired (K_m = 1100 μM and k_{cat} = 5 s^{-1}). The 220−225Th, Y99T, Q192E, and F174N mutants were constructed in the Gla domain-less forms (GD-FXa). The K_m values of all FXa mutants for SpFXa ranged from 65 to 80 μM. The Y99T and F174N mutants are gain-of-function mutants which show a preference for the activated protein C-specific chromogenic substrate SpPCa, as characterized previously (*31*, *35*). The K_m values of Y99T and F174N for SpPCa were 220 and 440 μM, respectively.

Table 1: K_I Values for the Inhibition of FXa Mutants by rTAP[a]

	K_I (pM)	$-\Delta G°_b$ (kJ/mol)	$\Delta\Delta G°_b$ (kJ/mol)
wild-type FXa	236 ± 29	54.9	−
GD-FXa	380 ± 33	53.7	1.2
E36Q	458 ± 46	53.3	1.6
E37Q	294 ± 31	54.4	0.5
E39Q	253 ± 50	54.7	0.2
Q61A	371 ± 28	53.8	1.1
K62E	312 ± 22	54.2	0.7
R63E	270 ± 34	54.6	0.3
R93A	270 ± 44	54.6	0.3
K96A	105 ± 14	56.9	−2.0
E97A	545 ± 49	52.8	2.0
R143A	25900 ± 2100	43.3	11.6
K147A	212 ± 11	55.2	−0.3
R150A	517 ± 79	53.0	1.9
R154A	708 ± 64	52.2	2.7
220−225Th	291400 ± 38800	37.3	17.6
Q192E	122 ± 22	56.6	−1.7
Y99T	14800 ± 1100	44.7	10.2
F174N	197300 ± 5500	38.2	16.7

[a] The K_I values for the rTAP inhibition of FXa derivatives were determined by a discontinuous assay at room temperature as described in Materials and Methods. With the exception of R143A, 220−225Th, Y99T, and F174N for which eq 2 was used to calculate K_I values, eq 1 was utilized to calculate the values in all cases. All values are averages of at least two or three independent measurements ± the standard error.

Inhibition of FXa Derivatives by rTAP. Previous studies have indicated that rTAP is a competitive, slow- and tight-binding inhibitor of FXa with a K_I of ∼180 pM (*10*, *12*). Using eq 1 for the tight-binding inhibitors, a similar K_I value of 236 pM was obtained for the rTAP inhibition of FXa in this study (Table 1). The removal of the Gla domain from FXa appears to slightly impair the affinity of the protease for rTAP, as evidenced by a 1.6-fold elevation in the K_I value [Table 1 and Figure 1A (○)]. Four mutants (R143A, F174N, Y99T, and 220−225Th) exhibited dramatic impairments in their interaction with rTAP (Figure 1B for F174N and 220−225Th, and Table 1); however, all other mutants efficiently bound to the inhibitor, though the K_I values with certain mutants were either slightly improved (K96A and Q192E; Figure 1A, ● shown for Q192E only) or impaired (E36Q, E97A, R150A, and R154A). To compare the contribution of each mutant residue in binding to the inhibitor, the K_I values were determined and converted to the free energy of binding ($\Delta G°_b$), and the difference between the values for the wild type and the mutant ($\Delta\Delta G°_b$) was calculated and presented in Table 1. Analysis of the data indicated that each one of the four mutants with the greatest impairment in K_I exhibited a loss of binding energy from ∼10 to ∼18 kJ/mol. The mutagenesis effect with most other mutants was minor, with E36Q, E97A, R150A, and R154A exhibiting a 1.6−2.7 kJ/mol decrease and K96A and Q192E a 1.7−2 kJ/mol gain in binding energy (Table 1). Noting the dramatic impairments with R143A, 220−225Th, F174N, and Y99T mutants and the observation that the mechanism of inhibition of these mutants by rTAP was also changed from a slow- and tight-binding inhibition mechanism to a reversible-type inhibition (see below), we calculated the K_I values for these mutants under pseudo-first-order conditions in the presence of an excess inhibitor with eq 2 as described in Materials and Methods.

Slow-Binding Kinetic Approach. To determine the mechanism by which rTAP inhibits the FXa mutants, a series of progress curves was generated by continuously monitoring the rate of cleavage of chromogenic substrates (SpFXa for all mutants with the exception of SpPCa for the Y99T and F174N mutants) by mutant enzymes in the presence of increasing concentrations of the inhibitor under pseudo-first-order conditions. As shown in Figure 2A, rTAP inhibited GD-FXa by a slow- and tight-binding inhibition mechanism, similar to that described in the past for wild-type FXa (*12*, *13*). The k_{obs} values for the rTAP inhibition of GD-FXa at different concentrations of rTAP were determined by fitting data to the slow-binding equation (eq 3) as described previously (*12*). To differentiate between the inhibition mechanisms of Schemes 1 and 2, the k_{obs} values were plotted as a function of rTAP concentration. The results indicated that rTAP inhibits GD-FXa according to Scheme 1 under the experimental conditions described in the legend of Figure 2. This was evidenced by the observation that the k_{obs} values exhibited a linear dependence on the inhibitor concentration as shown in Figure 2B. Thus, analysis of data according to eqs 4 and 5 yielded the following values: $k_1 = (1.2 \pm 0.04) \times 10^6$ M^{-1} s^{-1}, $k_{-1} = (6.4 \pm 0.8) \times 10^{-4}$ s^{-1}, and K_I = 533.3 pM. The corresponding values for the full-length FXa were as follows: $k_1 = (1.2 \pm 0.02) \times 10^6$ M^{-1} s^{-1}, $k_{-1} = (2.7 \pm 0.4) \times 10^{-4}$ s^{-1}, and K_I = 225.0 pM. These results suggest that, relative to that of FXa, k_{-1} for GD-FXa is increased ∼2-fold which accounts for the slight difference

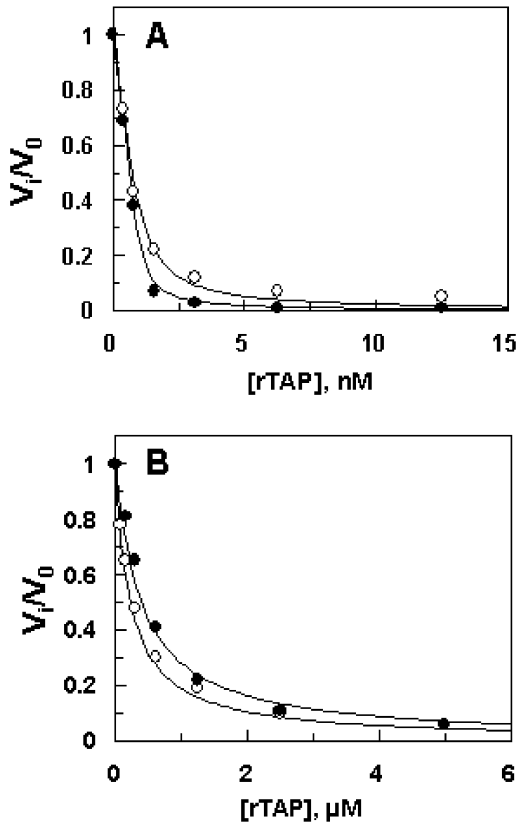

FIGURE 1: Inhibition of GD-FXa derivatives by rTAP. (A) Wild-type (○) or Q192E (●) GD-FXa (0.5 nM each) was incubated with rTAP (0−15 nM) in TBS/Ca^{2+}, and the K_I values at equilibrium were determined from the remaining activity of enzymes using the tight binding equation (eq 1) as described in Materials and Methods. (B) Same as panel A except that the K_I values for the F174N (○) and 220−225Th (●) mutants at equilibrium were determined under pseudo-first-order conditions using eq 2. Solid lines in panels A and B are the best fit of kinetic data to eqs 1 and 2, respectively.

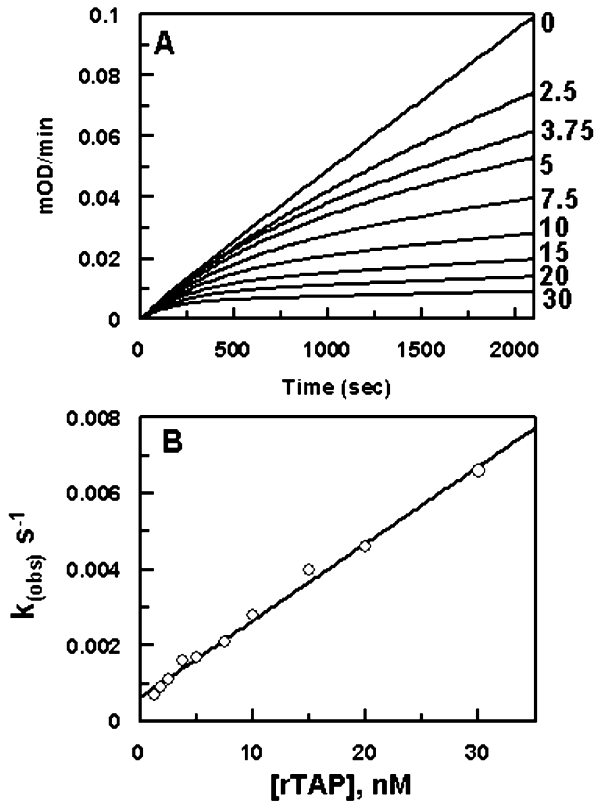

FIGURE 2: Progress curves for rTAP inhibition of GD-FXa. (A) GD-FXa (0.1 nM) was added to wells of a 96-well assay plate containing 400 μM SpFXa and varying concentrations of rTAP (from 0 to 30 nM, solid lines from top to bottom) in TBS/Ca^{2+}. The k_{obs} values at each inhibitor concentration were determined by fitting data to eq 3 as described in Materials and Methods. (B) The k_{obs} values, determined in panel A, were fitted to eq 4, a relationship describing the linear dependence of k_{obs} values on the concentrations of the inhibitor according to Scheme 1: $k_1 = (1.2 \pm 0.04) \times 10^6$ M^{-1} s^{-1}, $k_{-1} = (6.4 \pm 0.8) \times 10^{-4}$ s^{-1}, and $K_I = 533.3$ pM.

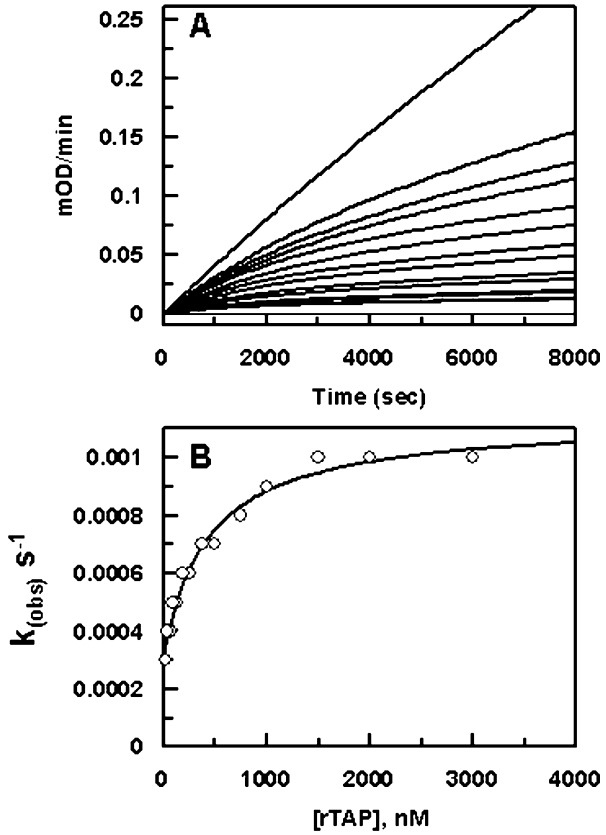

FIGURE 3: Progress curves for rTAP inhibition of the R143A mutant of FXa. (A) The FXa mutant (0.1 nM) was added to wells of a 96-well assay plate containing 400 μM SpFXa and varying concentrations of rTAP (from 0 to 3000 nM, solid lines from top to bottom) in TBS/Ca^{2+}. The k_{obs} values at each inhibitor concentration were determined by fitting the data to eq 3. (B) The k_{obs} values, determined in panel A, were fitted to eq 6, a relationship describing the hyperbolic dependence of k_{obs} values on the concentrations of the inhibitor according to Scheme 2: $k_2 = (8.2 \pm 0.4) \times 10^{-4}$ s^{-1}, $k_{-2} = (3.2 \pm 0.3) \times 10^{-4}$ s^{-1}, initial $K_i = 86.4$ nM, and final $K_I = 24.1$ nM.

in the K_I of the inhibition. The K_I values determined by this method of analysis correlate well with the same values determined for both FXa and GD-FXa using eq 1, supporting the validity of the measurements (Table 1). Previously, similar values for the rTAP inhibition of FXa ($k_1 = 2.85 \times 10^6$ M^{-1} s^{-1} and $k_{-1} = 5.5 \times 10^{-4}$ s^{-1}) have been reported by others (*12*); thus, rTAP interacts with GD-FXa with similar kinetics, and the slight decrease in binding energy is due to an ~2-fold elevated dissociation rate constant (k_{-1}).

The slow-binding kinetic approach was also employed to study the mechanism by which rTAP interacts with the FXa mutants. In the case of interaction with the R143A mutant where the K_I has been elevated 110-fold, analysis of the inhibition progress curves at different concentrations of rTAP suggested that, like the interaction with wild-type FXa, a slow inhibition mechanism accounts for the interaction of the inhibitor with the mutant protease. However, unlike the inhibition of the wild type, a steady-state velocity for the mutant protease approached at a much delayed time point (compare Figure 3A with Figure 2A). Interestingly, unlike that of the wild type, k_{obs} values increased hyperbolically as a function rTAP concentration, suggesting that the inhibitor interacts with the mutant protease according to Scheme 2 (Figure 3B). Thus, analysis of data according to eqs 6 and 7 yielded the following values: $k_2 = (8.2 \pm 0.4) \times 10^{-4}$ s^{-1}, $k_{-2} = (3.2 \pm 0.3) \times 10^{-4}$ s^{-1}, initial $K_i = 86.4$ nM, and final $K_I = 24.1$ nM. Thus, there was an only ~2.5-fold difference between the association and dissociation rate constants for the isomerization of the protease−inhibitor complex in the second step of the interaction, possibly explaining the basis for the delay in approaching the steady-state velocity by the mutant enzyme. The K_I value for the R143A mutant could also be determined under pseudo-first-order conditions using eq 2, yielding a similar K_I value of ~26 nM (Table 1) suggesting that the interaction of rTAP with the mutant protease has been considerably weakened.

Analysis of the progress curves for the rTAP inhibition of Y99T, F174N, and the sodium-binding 220−225Th loop mutants, which exhibited the greatest decrease in binding energy, provided no evidence for a slow-type inhibition mechanism for the interaction of the inhibitor with either mutant of FXa (Figure 4 shown for Y99T and 220−225Th mutants only). These results suggested that rTAP establishes equilibrium with these mutants on a time scale that is rapid with respect to the turnover rate of the enzymatic reactions, and thus, K_I values could be determined in the presence of excess inhibitor from the nonlinear regression analysis of kinetic data according to eq 2 (Table 1). Taken together, these results suggest that the interactions of rTAP with residues of the aryl binding pocket, autolysis loop, and the

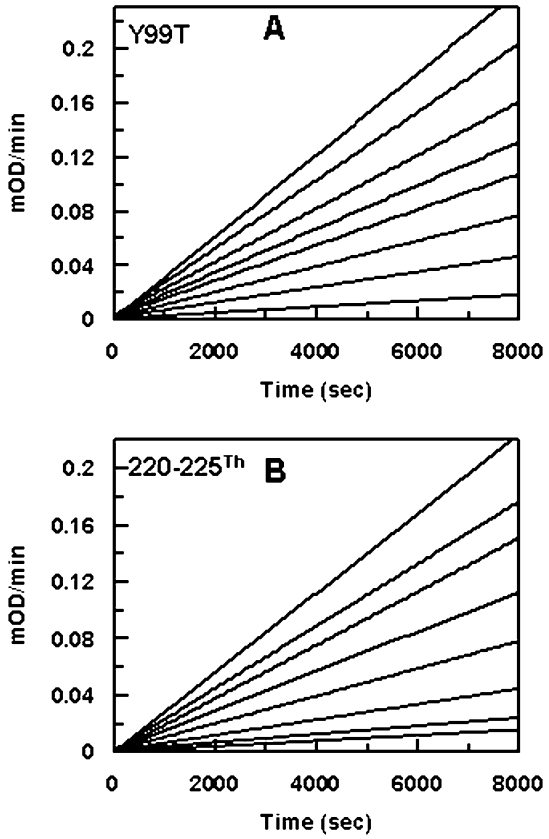

FIGURE 4: Progress curves for rTAP inhibition of Y99T and 220−225Th mutants. (A) The Y99T mutant (0.1 nM) was added to wells of a 96-well assay plate containing 400 μM SpPCa and varying concentrations of rTAP (from 0 to 500 nM, solid lines from top to bottom) in TBS/Ca^{2+}. (B) The 220−225Th mutant (5 nM) was added to wells of a 96-well assay plate containing 400 μM S2765 and varying concentrations of rTAP (from 0 to 10 μM, solid lines from top to bottom) in TBS/Ca^{2+}. The amidolytic activity in both panels remained linear for the duration of the measurements (2 h). The K_I values were determined by fitting data to eq 2, as described in Materials and Methods.

Na^+-binding 220 loop account for its high specificity for FXa and its ability to inhibit the protease by a slow- and tight-binding inhibition mechanism.

DISCUSSION

The results presented above suggest that rTAP must interact with at least three specific sites of FXa to inhibit the protease via a characteristic slow- and tight-binding inhibition mechanism. All three rTAP interactive sites on FXa have unique amino acid residues which are not conserved in other coagulation proteases, accounting for the high specificity of the interaction of FXa with the inhibitor. The unique amino acid residues include the two aryl binding pocket residues, Tyr^{99} and Phe^{174}, autolysis loop residue Arg^{143}, and the three basic residues of the sodium-binding 220−225 loop. The K_I values for the interaction of rTAP with mutants of all three sites were dramatically impaired. On the basis of the criteria established by Morrison and Walsh for defining the slow- and tight-binding inhibitors (*32*), the mechanism of inhibition of the mutant proteases by rTAP was also changed from a slow- and tight-binding type to a reversible type, suggesting that the mutant residues play a pivotal role in the specificity of the inhibitor interaction. Noting that the mutant residues of all three

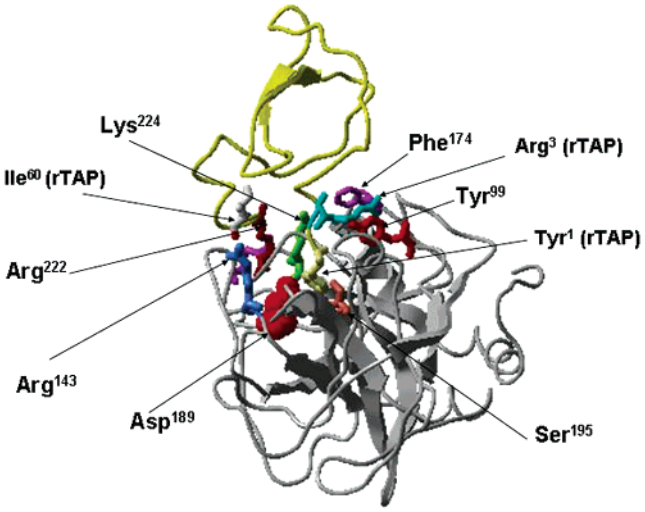

FIGURE 5: Crystal structure of the catalytic domain of bovine FXa in complex with rTAP. The P1 Tyr^1, P3 Arg^3, and C-terminal end residue Ile^{60} of rTAP (yellow) are denoted with arrows. The S1 primary binding site Asp^{189} and the catalytic Ser^{195} are shown in the middle of the protease domain (gray). The NH_2 group of the side chain of the autolysis loop residue Arg^{143} (blue) is 2.7 Å from the carboxyl oxygen atom of the rTAP residue, Ile^{60}. The side chain of P3 Arg^3 of the inhibitor is sandwiched between the two aromatic rings of Tyr^{99} and Phe^{174} in the aryl binding pocket of FXa. The side chains of Arg^{222} and Lys^{224}, located on the back of the protease domain, are denoted with arrows. The side chain of Lys^{223}, which is not labeled in the diagram and points away from the inhibitor, is shown in purple behind Arg^{222}. The coordinates (Protein Data Bank entry 1KIG) were used to prepare the figure (*15*).

interactive sites are located on different loops, we find their contribution to binding energy is likely to be additive. However, further study with a construct containing mutations in all three sites is required to validate this prediction. The relative orientation of the side chains of the mutant residues in the three-dimensional structure of bovine FXa in complex with rTAP is presented in Figure 5 (*15*). All of the residues, which were determined to be critical for the interaction of rTAP with human FXa, are also conserved in bovine FXa. Thus, the structural data can be utilized to interpret the mutagenesis data with human FXa. As shown in Figure 5, the hydrophobic side chain of Arg^3 is stabilized in the aryl binding pocket by the aromatic rings of Tyr^{99} and Phe^{174}, explaining the dramatic impairment observed in the binding of both mutants with the inhibitor. Structural data have also indicated that the guanidinium group of Arg^3 makes a salt bridge with the side chain of Glu^{97} to neutralize the charge of the basic residue in the hydrophobic aryl binding pocket of the protease (*15*). However, the observation that the K_I values for the inhibition of Y99T and F174N, but not E97A, were severely impaired suggests that most of the binding energy of the interaction of Arg^3 with the pocket is mediated by the hydrophobic interaction of its side chain with the aryl binding pocket, but not its guanidinium group interacting with Glu^{97}. Moreover, the structural data have indicated that P1 Tyr^1 of rTAP binds to the S1 specificity pocket of FXa with its side chain hydroxyl group hydrogen bonding to the primary S1 specificity pocket (Asp^{189}), and Asn^2 hydrogen bonding to Gln^{192} of the protease (*15*). Results of other previous mutagenesis experiments with rTAP are in agreement with this mode of S1−P1 interaction; however, the observation that there was a 1.7 kJ/mol increase in the

binding energy of the interaction of rTAP with the Q192E mutant suggests that Gln^{192} does not play a role in the specificity of the protease−inhibitor interaction. It should be noted that such differences between the structural and mutagenesis data may also be attributable to possible differences in the mode of interaction of rTAP with either human or bovine FXa.

Previous structural data have indicated that FXa utilizes a similar mechanism to interact with DX-9065a, a small and specific active site-directed inhibitor of the protease (*38*). Thus, it has been noted that the interaction of DX-9065a with both hydrophobic residues of the aryl binding pocket of FXa also makes a marked contribution to the binding energy of the inhibitor interaction (*39*). Moreover, similar to the interaction with rTAP, neither Glu^{97} nor Gln^{192} of FXa plays a significant role in the DX-9065a recognition (*39*). On the other hand, Gln^{192} but not Tyr^{99} has been shown to play a key role in the specificity of the interaction of FXa with TFPI (*30*, *31*). Therefore, the determinants of the inhibitor specificity in the active site pocket of FXa are the same for both rTAP and DX-9065a, but different for TFPI.

In addition to the catalytic pocket, the structural data have further indicated that two acidic domains at the C-terminal end of rTAP interact with two basic exosites of bovine FXa, thus forming salt bridges or hydrogen bonds with Arg^{143}, Lys^{147}, and Arg^{149} of the autolysis loop and Arg^{222} and Lys^{224} of the sodium-binding loop (*15*) (Figure 5). The autolysis loop of human FXa, from residue 143 to 154, has four basic residues: Arg^{143}, Lys^{147}, Arg^{150}, and Arg^{154}. The mutagenesis data presented above suggest that only Arg^{143} of human FXa is critical for the interaction with rTAP. Although the interaction of rTAP with the Arg^{143} mutant exhibited slow-binding type kinetics, the association rate constant for the isomerization of the protease−inhibitor complex in the second step of the reaction (*13*) was dramatically impaired. Examination of the crystal structure of the bovine FXa−rTAP complex suggests that the NH_2 group of Arg^{143} is within salt bridging distance (2.7 Å) of the C-terminal carboxyl oxygen atom of Ile^{60} (Figure 5). On the basis of our mutagenesis data, we believe that this interaction primarily accounts for the binding energy of the interaction of the autolysis loop with the inhibitor. The mutagenesis data suggest that no productive interaction occurs between rTAP and Lys^{147} of human FXa since the binding energy with the K147A mutant was not impaired, but slightly improved. However, the data in Table 1 suggest that both Arg^{150} and Arg^{154} slightly contribute to the binding energy of the inhibitor interaction. Unlike the important role Arg^{143} plays in the interaction of FXa with rTAP, previous mutagenesis data have indicated that neither of the basic residues of the autolysis loop plays a significant role in the interaction of protease with TFPI (*34*), thus suggesting that, like differences in the active site binding specificity, determinants of the exosite binding specificity of the two inhibitors are also different.

In agreement with the structural data, the results of this study implied an important role for the sodium-binding 220 loop in the interaction of FXa with rTAP. Unfortunately, however, the mutagenesis of this loop also dramatically impaired the activity and sodium binding properties of the mutant protease, thus complicating the interpretation of the kinetic data. Another FXa mutant in which all three basic residues (Arg^{222}, Lys^{223}, and Lys^{224}) were substituted with Ala exhibited a similar defect in its amidolytic activity toward S2765 and its interaction with rTAP (data not shown). Thus, it is not possible to assign a specific role for the basic residues of the sodium loop in interaction with rTAP solely by the mutagenesis data presented above. Examination of the relative orientations of the side chains of three basic residues of the sodium-binding loop suggests that only Arg^{222} and Lys^{224} can interact with the inhibitor since the ammonium group of Lys^{223} is pointing away from the inhibitor (Figure 5). It should be noted that, like the interaction with rTAP, the affinity of the sodium-binding loop mutants for interaction with TFPI and antithrombin was also dramatically impaired. Thus, the severe defect in the binding properties of the mutant with rTAP could also be caused by a loss of interaction with the subsite residues of the protease, particularly with the S1 primary specificity pocket, which has been demonstrated to be in an allosteric linkage with the sodium-binding loop of the protease (*40*, *41*). It follows, therefore, that only in the context of the structural data can the results of this study assign a specific role for the interaction of rTAP with basic residues of this loop. The results nevertheless suggest that, as for other coagulation proteases (*42*), the 220−225 loop plays a decisive role in the structure and catalytic function of FXa.

ACKNOWLEDGMENT

I thank Audrey Rezaie for proofreading of the manuscript.

REFERENCES

1. Mann, K. G., Jenny, R. J., and Krishnaswamy, S. (1988) Cofactor proteins in the assembly and expression of blood clotting enzyme complexes, *Annu. Rev. Biochem. 57*, 915−956.
2. Rosing, J., Tans, G., Govers-Riemslag, J. W. P., Zwaal, R. F. A. Z., and Hemker, H. C. (1980) The role of phospholipids and factor Va in the prothrombinase complex, *J. Biol. Chem. 255*, 274−283.
3. Damus, P. S., Hicks, M., and Rosenberg, R. D. (1973) Anticoagulant action of heparin, *Nature 246*, 355−357.
4. Olson, S. T., and Björk, I. (1992) Regulation of thrombin by antithrombin and heparin cofactor II, in *Thrombin: Structure and Function* (Berliner, L. J., Ed.) pp 159−217, Plenum Press, New York.
5. Han, X., Fiehler, R., and Broze, G. J., Jr. (2000) Characterization of the protein Z-dependent protease inhibitor, *Blood 96*, 3049−3055.
6. Broze, G. J., Jr., Girard, T. J., and Novotny, W. F. (1990) Regulation of coagulation by a multivalent Kunitz-type inhibitor, *Biochemistry 29*, 7539−7546.
7. Jin, L., Abrahams, J., Skinner, R., Petitou, M., Pike, R. N., and Carrell, R. W. (1997) The anticoagulant activation of antithrombin by heparin, *Proc. Natl. Acad. Sci. U.S.A. 94*, 14683−14688.
8. Huang, Z.-F., Wun, T.-C., and Broze, G. J., Jr. (1993) Kinetics of factor Xa inhibition by tissue factor pathway inhibitor, *J. Biol. Chem. 268*, 26950−26955.
9. Burgering, M. J. M., Orbons, L. P. M., van der Doelen, A., Mulders, J., Theunissen, H. J. M., Grootenhuis, P. D. J., Bode, W., Huber, R., and Stubbs, M. T. (1997) The second Kunitz domain of human tissue factor pathway inhibitor: Cloning, structure determination and interaction with factor Xa, *J. Mol. Biol. 269*, 395−407.
10. Vlasuk, G. P. (1993) Structural and functional characterization of tick anticoagulant peptide (TAP): a potent and selective inhibitor of blood coagulation factor Xa, *Thromb. Haemostasis 70*, 212−216.
11. Mao, S.-S., Przysiecki, C. T., Krueger, J. A., Cooper, C. M., Lewis, S. D., Joyce, J., Lellis, C., Garsky, V. M., Sardana, M., and Shafer, J. A. (1998) Selective inhibition of factor Xa in the prothrombinase complex by the carboxyl-terminal domain of antistasin, *J. Biol. Chem. 273*, 30086−30091.

12. Jordan, S. P., Waxman, L., Smith, D. E., and Vlasuk, G. P. (1990) Reaction pathway for inhibition of blood coagulation factor Xa by tick anticoagulant peptide, *Biochemistry 29*, 11095−11100.
13. Jordan, S. P., Mao, S.-S., Lewis, S. D., and Shafer, J. A. (1992) Reaction pathway for inhibition of blood coagulation factor Xa by tick anticoagulant peptide, *Biochemistry 31*, 5374−5380.
14. Betz, A., Vlasuk, G. P., Bergum, P. W., and Krishnaswamy, S. (1997) Selective inhibition of the prothrombinase complex: Factor Va alters macromolecular recognition of a tick anticoagulant peptide mutant by factor Xa, *Biochemistry 36*, 181−191.
15. Wei, A., Alexander, R. S., Duke, J., Ross, H., Rosenfeld, S. A., and Chang, C.-H. (1998) Unexpected binding mode of tick anticoagulant peptide complexed to bovine factor Xa, *J. Mol. Biol. 283*, 147−154.
16. Schechter, I., and Berger, A. (1967) On the size of the active site in proteases. I. Papain, *Biochem. Biophys. Res. Commun. 27*, 157−162.
17. Bode, W., Mayr, I., Baumann, U., Huber, R., Stone, S. R., and Hofsteenge, J. (1989) The refined 1.9 Å crystal structure of human α-thrombin: interaction with D-Phe-Pro-Arg chloromethylketone and significance of the Tyr-Pro-Pro-Trp insertion segment, *EMBO J. 8*, 3467−3475.
18. Dang, Q. D., and Di Cera, E. (1996) Residue 225 determines the Na^+-induced allosteric regulation of catalytic activity in serine proteases, *Proc. Natl. Acad. Sci. U.S.A. 93*, 10653−10656.
19. Grutter, M. G., Priestle, J. P., Rahuel, J., Grossenbacher, H., Bode, W., Hofsteenge, J., and Stone, S. R. (1990) Crystal structure of the thrombin-hirudin complex: a novel mode of serine protease inhibition, *EMBO J. 9*, 2361−2365.
20. Rydel, T. J., Tulinsky, A., Bode, W., and Huber, R. (1991) Refined structure of the hirudin-thrombin complex, *J. Mol. Biol. 221*, 583−601.
21. Qiu, X., Padmanabhan, K. P., Carperos, V. E., Tulinsky, A., Kline, T., Maraganore, J. M., and Fenton, J. W., II (1992) Structure of the hirulog 3-thrombin complex and nature of the S′ subsites of substrates and inhibitors, *Biochemistry 31*, 11689−11697.
22. Furie, B., Bing, D. H., Feldman, R. J., Robison, D. J., Burnier, J. F., and Furie, B. C. (1982) Computer-generated models of blood coagulation factor Xa, factor IXa and thrombin based upon structural homology with other serine proteases, *J. Biol. Chem. 257*, 3875−3882.
23. Stubbs, M. T., and Bode, W. (1993) A player of many parts: The spotlight falls on thrombin's structure, *Thromb. Res. 69*, 1−58.
24. Baugh, R. J., Dickinson, C. D., Ruf, W., and Krishnaswamy, S. (2000) Exosite interactions determine the affinity of factor X for the extrinsic Xase complex, *J. Biol. Chem. 275*, 28826−28833.
25. Anderson, P. J., Nesset, A., Dharmawardana, K. R., and Bock, P. E. (2000) Role of proexosite I in factor Va-dependent substrate interactions of prothrombin activation, *J. Biol. Chem. 275*, 16435−16442.
26. Chen, L., Yang, L., and Rezaie, A. R. (2003) Proexosite on prothrombin is a factor Va-dependent recognition site for the prothrombinase complex, *J. Biol. Chem. 278*, 27564−27569.
27. Gale, A. J., Tsavaler, A., and Griffin, J. H. (2002) Molecular characterization of an extended binding site for coagulation factor Va in the positive exosite of activated protein C, *J. Biol. Chem. 277*, 28836−28840.
28. Friedrich, U., Nicolaes, G. A. F., Villoutreix, B. O., and Dahlbäck, B. (2001) Secondary substrate-binding exosite in the serine protease domain of activated protein C important for cleavage at Arg-506 but not at Arg-306 in factor Va, *J. Biol. Chem. 276*, 23105−23108.
29. Kolkman, J. A., and Mertens, K. (2000) Surface-loop residue Lys316 in blood coagulation factor IX is a major determinant for factor X but not antithrombin recognition, *Biochem. J. 350*, 701−707.
30. Rezaie, A. R., and Esmon, C. T. (1996) Molecular basis of residue 192 participation in determination of coagulation protease specificity, *Eur. J. Biochem. 242*, 477−484.
31. Rezaie, A. R. (1996) Role of residue 99 at the S2 subsite of factor Xa and activated protein C in enzyme specificity, *J. Biol. Chem. 271*, 23807−23814.
32. Morrison, J. F., and Walsh, C. T. (1988) The behavior and significance of slow-binding enzyme inhibitors, *Adv. Enzymol. Relat. Areas Mol. Biol. 61*, 201−301.
33. Rezaie, A. R., Neuenschwander, P. F., Morrissey, J. H., and Esmon, C. T. (1993) Analysis of the functions of the first epidermal growth factor-like domain of factor X, *J. Biol. Chem. 268*, 8176−8180.
34. Manithody, C., Yang, L., and Rezaie, A. R. (2002) Role of basic residues of the autolysis loop in the catalytic function of factor Xa, *Biochemistry 41*, 6780−6788.
35. Monnaie, D., Arosio, D., Griffon, N., Rose, T., Rezaie, A. R., and Di Cera, E. (2000) Identification of a binding site for quaternary amines in factor Xa, *Biochemistry 39*, 5349−5354.
36. Rezaie, A. R., He, X., and Esmon, C. T. (1998) Thrombomodulin increases the rate of thrombin inhibition by BPTI, *Biochemistry 37*, 693−699.
37. Tian, W. X., and Tsou, C. L. (1982) Determination of the rate constant of enzyme modification by measuring the substrate reaction in the presence of the modifier, *Biochemistry 21*, 1028−1032.
38. Brandstetter, H., Kuhne, A., Bode, W., Huber, R., von der Saal, W., Wirthensohn, K., and Engh, R. A. (1996) X-ray structure of active site-inhibited clotting factor Xa. Implications for drug design and substrate recognition, *J. Biol. Chem. 271*, 29988−29992.
39. Rezaie, A. R. (2003) DX-9065a inhibition of factor Xa and the prothrombinase complex: mechanism of inhibition and comparison with therapeutic heparins, *Thromb. Haemostasis 89*, 112−121.
40. Rezaie, A. R., and He, X. (2000) Sodium binding site of factor Xa: Role of sodium in the prothrombinase complex, *Biochemistry 39*, 1817−1825.
41. Camire, R. M. (2002) Prothrombinase assembly and S1 site occupancy restore the catalytic activity of FXa impaired by mutation at the sodium-binding site, *J. Biol. Chem. 277*, 37863−37870.
42. Guinto, E. R., Caccia, S., Rose, T., Futterer, K., Waksman, G., and Di Cera, E. (1999) Unexpected crucial role of residue 225 in serine proteases, *Proc. Natl. Acad. Sci. U.S.A. 96*, 1852−1857.

BI036177Y